Area-specific thalamocortical synchronization underlies the transition from motor planning to execution

Abdulraheem Nashef[a,b,c], Rea Mitelman[a,b,c], Ran Harel[d], Mati Joshua[c], and Yifat Prut[a,b,c,1]

[a]Department of Medical Neurobiology, Hadassah Medical School, The Hebrew University, 9112102 Jerusalem, Israel; [b]Institute of Medical Research Israel-Canada, Hadassah Medical School, The Hebrew University, 9112102 Jerusalem, Israel; [c]The Edmond and Lily Safra Center for Brain Sciences, The Hebrew University, 9190401 Jerusalem, Israel; and [d]Department of Neurosurgery, Sheba Medical Center, 5262000 Tel Aviv, Israel

Edited by Peter L. Strick, University of Pittsburgh, Pittsburgh, PA, and approved January 5, 2021 (received for review June 21, 2020)

We studied correlated firing between motor thalamic and cortical cells in monkeys performing a delayed-response reaching task. Simultaneous recording of thalamocortical activity revealed that around movement onset, thalamic cells were positively correlated with cell activity in the primary motor cortex but negatively correlated with the activity of the premotor cortex. The differences in the correlation contrasted with the average neural responses, which were similar in all three areas. Neuronal correlations reveal functional cooperation and opposition between the motor thalamus and distinct motor cortical areas with specific roles in planning vs. performing movements. Thus, by enhancing and suppressing motor and premotor firing, the motor thalamus can facilitate the transition from a motor plan to execution.

motor cortex | motor thalamus | nonhuman primates | cerebellum | movement initiation

Thalamocortical (TC) interactions play a critical role in all facets of brain functions. In the sensory systems, the thalamic nuclei act as a gate for incoming information. In the motor system, the synaptic contacts made by TC afferents are sparse (1, 2) but this pathway has been shown to make a significant functional contribution. In monkeys, for instance, blocking the outflow of cerebellar signals through the cerebellar-thalamocortical (CTC) pathway leads to delayed movement onset and impaired coordination (3). In mice trained on a forelimb reaching task, thalamic input was shown to drive motor cortical dynamics such that silencing the motor thalamus arrested reaching movements (4, 5). TC interactions can regulate motor cortical activity even before movement begins by maintaining prelicking preparatory activity in the anterolateral motor cortex of rodents through a positive feedback loop (6, 7). The diverse functional consequences of TC interactions can be accounted for, at least in part, by the different roles played by premotor and motor cortex in planning and executing motor actions (8–11). Hence, understanding the pattern and magnitude of TC interactions with different motor areas is necessary for elucidating thalamic contribution to motor cortical activity and motor behavior.

We simultaneously recorded the activity of identified thalamic and cortical cells which integrate cerebellar signals while monkeys performed a reaching task. We found that the TC correlation pattern was strongly affected by the targeted motor cortical site, expressing positive correlations with primary motor cortex but negative correlations with premotor cortex. These results suggest that TC interactions can either enhance or suppress cortical firing around movement onset. The positive correlations with the motor cortex which occur in parallel to the negative correlations with the premotor cortex may support the shift in activity between these two areas needed for switching from motor plan to motor action.

Results

Response Properties of Thalamic and Motor Cortical Neurons. We simultaneously recorded the activity of thalamic and motor cortical neurons (Fig. 1*A* and *SI Appendix*, Fig. S1) while monkeys performed a shoulder-elbow reaching task (Fig. 1*B*). Pinpointing thalamic cells that are part of nonsensory nuclei is challenging given the complex anatomy of the thalamic nuclei. To overcome this difficulty, we used single-pulse stimulation delivered to the superior cerebellar peduncle (SCP), which efficiently activates the CTC system (12, 13) and serves to tag motor thalamic and motor cortical neurons that integrate cerebellar signals (Fig. 1*C*). The response latencies of single cells confirmed the sequential activation of the thalamic and cortical areas in response to SCP stimulation ($\Delta t = 0.6$ to 1.3 ms; $P < 1.2 \times 10^{-9}$, Wilcoxon's rank-sum test; Fig. 1 *A* and *C* and *SI Appendix*, Fig. S2). We compared the activity of thalamic and motor cortical cells recorded during the same behavioral task from SCP-responsive cortical and thalamic sites (*Materials and Methods*). Consistent with previous studies (14, 15), the task-related activity of thalamic cells (motor thalamus; mTh) was similar in pattern to neurons recorded in the primary motor (M1) and premotor (PM) cortical areas (Fig. 2 *A*–*C*) but had higher baseline rate levels (Fig. 2*C*). By contrast, the fraction of directionally tuned thalamic cells (Fig. 2*D*) was lower compared with cortical neurons (Fig. 2*E*) and their tuning function was broader (Fig. 2*F*). Finally, over the entire population of recorded cells, we found a considerable overlap between the response onset times of the thalamic and cortical cells (Fig. 2*G*). Nonetheless, a paired comparison of response onset times across simultaneously recorded pairs of cortical and thalamic cells revealed an earlier onset of task-related activity in the motor thalamus compared with M1 but not PM (Fig. 2 *H* and *I*). Note, however, that the way onset time was calculated here included preparatory activity and was thus early relative to movement onset. Nonetheless, the same results (with later latency values) were obtained when measuring the

Significance

Thalamocortical interactions are a key component of normal brain functions both in sensory and motor areas. The fact that TC connectivity is excitatory has led to the suggestion that its main role is positively driving motor cortical activity. Here we show that the motor thalamus has contrasting, area-dependent interactions with cortical sites, such that it can either enhance or suppress motor cortical variability. The TC interactions with the primary motor vs. the premotor cortex put the motor thalamus in an ideal position to promote the transition from a motor plan to motor action and serve as an important driver of movement initiation.

Author contributions: Y.P. designed research; A.N., R.M., and R.H. performed research; A.N. and R.M. analyzed data; and A.N., M.J., and Y.P. wrote the paper.

The authors declare no competing interest.

This article is a PNAS Direct Submission.

[1]To whom correspondence may be addressed. Email: yifat.prut@mail.huji.ac.il.

This article contains supporting information online at https://www.pnas.org/lookup/suppl/doi:10.1073/pnas.2012658118/-/DCSupplemental.

Published February 1, 2021.

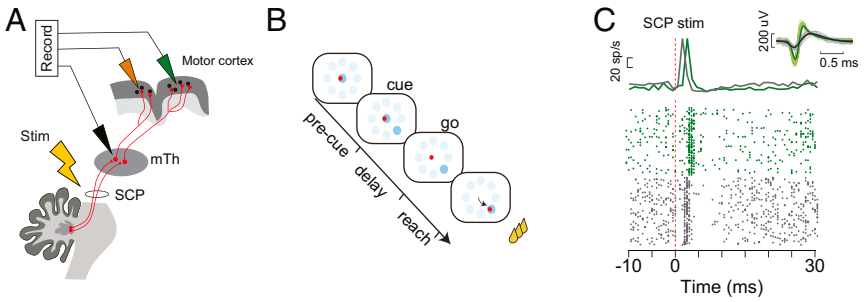

Fig. 1. Task schematic and SCP stimulation. (*A*) Illustration of the thalamocortical system and the experimental setup. Fibers from the deep cerebellar nuclei ascend via the superior cerebellar peduncle to contact neurons in the motor thalamus, which in turn send ascending fibers to the motor cortex. Recordings were made simultaneously in the motor thalamus and the motor cortex which includes the primary motor and premotor areas. Stimulations were applied through chronic stimulating electrodes implanted in the SCP. (*B*) The sequence of events composing a single trial included a precue period, cue onset (where one of eight equally distributed peripheral targets appeared), a delay period, and a go signal, after which the monkey had to acquire the target within a limited movement time. Correct performance resulted in a reward (a drop of applesauce). (*C*) Responses of simultaneously recorded thalamic (black raster plot) and motor cortical (green raster plot) cells to single-pulse SCP stimulation. Both raster plots are aligned around stimulation time ($t = 0$) indicated also by the vertical dashed line. (*C, Upper*) Two peristimulus time histograms, one for each cell. The neuronal waveforms (*Upper Right*) are depicted using 50 randomly selected waveforms (with an average waveform in bold).

onset time of movement-related activity (while ignoring motor preparation; *SI Appendix*, Fig. S3). Taken together, these results suggest that the motor thalamus provides the motor cortex with an early, albeit weakly tuned excitatory drive, which could potentially enhance the movement-related activity of motor cortical cells.

Area-Specific Thalamocortical Interactions around Movement Onset. The pattern of task-related activity of thalamic cells, their strictly excitatory synaptic contact with cortical neurons, and the loss of motor drive when thalamic input is silenced are considered evidence of the positive thalamic impact on motor cortical firing (4). However, averaged neural activity might not be an accurate predictor of neural interactions. Therefore, we estimated the efficacy of thalamic input in steering motor cortical activity by measuring the cell-to-cell thalamocortical interactions in relation to movement onset. This was done by calculating the joint peristimulus time histogram (jPSTH) which captures the modulation in the correlated firing of cells around selected events (16). The aligning event for computing these matrices was the time of movement onset ($t = 0$) and cell pairs were taken from somatotopically matching TC sites (*Materials and Methods*). We found that the pattern of TC correlation was highly dependent on the targeted cortical site. Specifically, there was a positive mTh–M1 correlation, particularly before movement onset (Fig. 3*A*; depicting the counts–predicted correlation matrix) in contrast to the asymmetric, positive–negative correlation profile for mTh–PM interactions (Fig. 3*B*). Finally, PM–M1 interactions were by and large weaker compared with the thalamocortical interactions, and showed a slightly negative correlation before movement onset and a brief positive correlation during movement (Fig. 3*C*).

Estimating the Directional Thalamocortical Interactions. The main diagonal of the jPSTH matrix captures the tendency for instantaneous cofiring of the tested sites. However, the diagonals above and below the main diagonal correspond to different positive or negative time lags of interactions between the two sites (*SI Appendix*, Fig. S4). Hence, we computed the directional time-resolved correlation by averaging bins above and below the main diagonal separately (Fig. 4 *A–C*). This calculation highlighted the differential TC interactions with M1 vs. PM neurons. For M1 sites, thalamic firing was positively correlated with subsequent M1 firing and vice versa specifically before movement onset (Fig. 4*A*). However, for PM sites, thalamic firing was negatively correlated with subsequent PM firing whereas PM firing was positively correlated with thalamic firing during movement (Fig. 4*B*). Finally, the M1–PM interactions were weaker and alternated between positive and negative values in both directions of the interactions (Fig. 4*C*). We tested the correlation for cortical cells that were SCP-responsive and found similar correlation patterns (*SI Appendix*, Fig. S5). This contrasting pattern of TC correlations with the M1 and PM cortex was preserved when we only considered triplets of simultaneously recorded mTh, M1, and PM cells such that the experimental conditions (and behavioral variability) were held constant in all pairwise interactions (Fig. 4*D*). To quantify the difference in thalamic interactions with M1 vs. PM, we defined a region of interest spanning 500 ms around movement onset and measured the average cofiring at this period for single TC pairs. We found that the distribution of values for mTh–M1 pairs was significantly different from the distribution for mTh–PM pairs (*SI Appendix*, Fig. S6; Wilcoxon rank-sum test, $P < 0.0007$). To test whether the observed correlation pattern is the result of difference in the tuning of M1 and PM cells in relation to mTh directionality, we selected a subset of M1–mTh cell pairs with a matching distribution of preferred direction differences (ΔPDs) to the distribution found for PM–mTh pairs and found that the correlation pattern of M1–mTh pairs remained similar (*SI Appendix*, Fig. S7). We then tested the relationship between cofiring, cortical site (M1 vs. PM), and ΔPD (*SI Appendix*, Fig. S8) and found a significant effect of site for both epochs (before and during movement) and significant effect of ΔPD solely before movement. Note, however, that there was no correlation between the ΔPD and the average cofiring that was found before or during movement (Kendall's correlation, $P > 0.05$; *SI Appendix*, Fig. S8). When selecting a subset of TC pairs with similar thalamic and cortical PDs ($|PD_{mTh} - PD_{cortex}| < 75°$), we obtained the same contrasting pattern of thalamocortical cofiring for M1 vs. PM (as found for the entire population), which differed from the PST predictor computed for these pairs (*SI Appendix*, Fig. S9). Finally, we used high-frequency stimulation (HFS) to the SCP to block transmission in the CTC pathway (3). During this time, the correlated firing between the motor thalamus and the motor cortex was lost (*SI Appendix*, Fig. S10), thus highlighting the cerebellar role in driving TC-correlated firing. Fig. 4*E* summarizes the results in a schematic diagram that shows the directional correlations at different epochs of the trial (also including the intraareal autocorrelation computed for each site as shown in *SI Appendix*, Fig. S11).

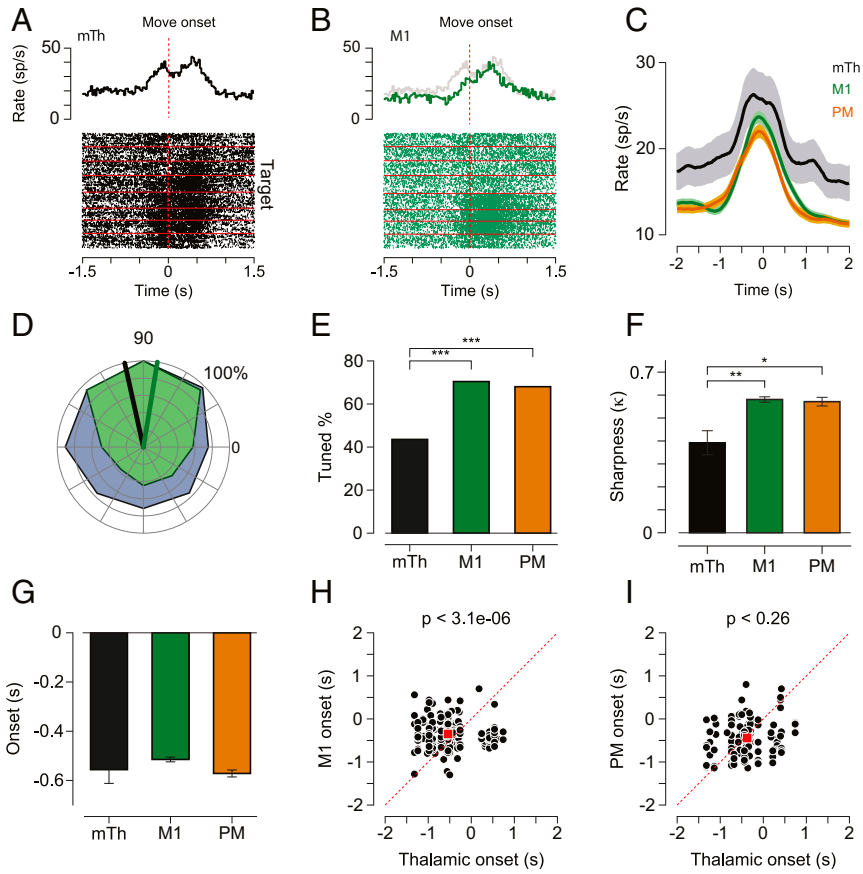

Fig. 2. Task-related activity of identified thalamic and cortical cells. (*A*) Example of task-related activity of a single thalamic cell aligned on movement onset (vertical red lines). Each line represents a single trial, and each dot corresponds to a single spike emitted by the cell. Trials are sorted by cue direction (1 through 8) and the horizontal red lines mark the transitions between different movement directions. (*A*, *Upper*) The perievent time histogram of the cell, computed by averaging the activity across all movement directions using a bin size of 25 ms. (*B*) Task-related activity of a single cortical neuron recorded simultaneously with the thalamic neuron shown in *A*. The PSTH of the thalamic cell in gray shading is depicted for comparison. (*C*) The mean firing rate (±SEM shading) of the three groups of cells recorded from the motor thalamus (black; $n = 78$ cells), M1 (green; $n = 1{,}734$ cells), and PM (orange; $n = 846$ cells). Activity was aligned on movement onset ($t = 0$). For directionally tuned cells, we computed the mean activity around the preferred direction (±1 target around the preferred target). For untuned cells, activity was averaged across all targets. (*D*) Example of tuning curves and preferred directions of thalamic (gray) and cortical (green) neurons recorded simultaneously. (*E*) The fraction of directionally tuned cells in each area (mTh: 43.6%; M1: 70.4%; PM: 68%; $^{***}P < 0.001$ using a χ^2 test with 1 degree of freedom). (*F*) Mean (±SEM) of the concentration parameter [Kappa (8, 26)] calculated from the Von Mises fit computed for all tuned cells for each of the Von Mises functions had a significant fit. The Kappa was correlated with the width of the tuning curve such that higher kappa values correspond to narrower tuning curves (mTh: 0.35 ± 0.03; M1: 0.53 ± 0.02; PM: 0.52 ± 0.04; Wilcoxon's rank-sum test, $^{***}P < 0.001$, $^{**}P < 0.01$, $^{*}P < 0.05$). (*G*) The mean onset time relative to movement onset computed for all three groups of neurons used to compute the average response profile shown in *C*. (*H*) Pairwise comparisons of the onset time computed for M1 neurons (*y* axis) and the corresponding thalamic neurons (*x* axis) that were recorded simultaneously. Each black circle indicates one simultaneous pair; the red rectangle represents the average of the pairwise comparisons and the red dashed line is the unity line ($x = y$). Red squares show the mean values (mean M1 onset = −0.35 ± 0.02 s; mTh onset = −0.54 ± 0.036 s; Wilcoxon's signed-rank test, $P = 3.1 \times 10^{-6}$). (*I*) Same as *H* but for PM neurons (average PM onset = −0.44 ± 0.04 s; mTh onset = −0.38 ± 0.045 s; $P = 0.26$).

Discussion

The results shown here suggest that the thalamic drive is involved in motor control via area-specific TC interactions that can enhance or suppress local cortical dynamics. The average activity and the tuning properties of individual thalamic cells indicate that this input is unlikely to provide a directionally tuned signal needed to drive downstream elements. Nonetheless, recording simultaneously thalamic and cortical activity revealed specific task-related TC interactions which are otherwise masked. This approach enabled us to show that thalamic signals are sufficiently strong to entrain the firing of motor cortical cells in a trial-by-trial manner. Specifically, when thalamic signals preceded cortical firing they had a positive impact on motor cortical firing and a strong negative impact on PM activity. Moreover, the fact that the correlated firing was abolished when information flow through the TC pathway was impaired may suggest that the thalamic control of cortical activity is stronger than the cortical feedback over thalamic activity which was insufficient to maintain TC correlation. We therefore conclude that the reciprocal TC interactions are nonsymmetric in strength as was previously suggested (17).

The positive feedback loop found between mTh and M1 is congruent with the anatomy of the system, but the negative correlation between mTh and the premotor cortex is less intuitive and may require an inhibitory link between the thalamic and premotor activity. Based on this study, we can only speculate on the possible mechanisms which could contribute to this inverse correlation pattern. Previously, we showed that the cortical response to CTC activation is dominated by strong inhibition which is consistent with a feedforward inhibition circuitry (12, 18, 19). Hence, local motor cortical inhibition triggered by the thalamic volley may inhibit PM activity in a manner which overrides the

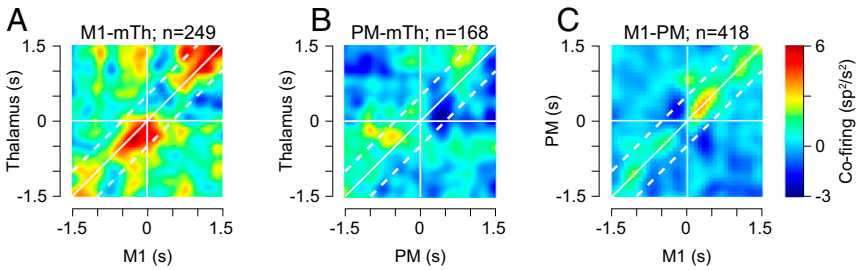

Fig. 3. Site-specific modulation of TC interactions. (*A*) jPSTH computed between the thalamic (*y* axis) and M1 (*x* axis) neurons for trials performed toward the preferred direction of the thalamic neurons. The plotted matrix depicts the differences between the actual count matrix and the predicted count matrix computed based on the PSTH of the cells. Time 0 corresponds to movement onset, and the diagonal depicts the zero-lag interunit interactions. The *z* axis corresponds to the color-coded covariance values (sp^2/s^2). Vertical and horizontal white lines correspond to movement onset time. The dashed diagonal lines highlight the data used to compute the mean time-resolved correlation values. (*B*) Same as in *A* but for mTh–PM cell pairs. (*C*) Same as in *A* but for M1–PM cell pairs. Here, for each pair the preferred direction for computing the matrices was randomly selected as the PD of either cell.

weaker excitation the PM receives via direct thalamic inputs (12, 20). Alternatively, the contrasting thalamic correlation with M1 vs. PM may reflect intrathalamic inhibitory interactions between different nuclei which are both part of the motor TC system (i.e., cerebellar vs. basal ganglial receiving nuclei) but have different distributions of terminations in the frontal lobe. It was shown that the cortical projections of the cerebellar receiving motor thalamus are biased toward M1 whereas the basal ganglial receiving thalamus projects more strongly to premotor areas (21). In this study, we focused on the cerebellar receiving thalamus, and therefore the negative correlation with the PM cortex suggests lateral inhibition between the two thalamic nuclei either directly (via interneurons) or via reticular collaterals (22–24). Nonetheless, more data are necessary to differentiate between direct and indirect effects thalamocortical fibers have on the different cortical areas. Overall, the findings suggest that during performance of well-practiced movements, the main contribution of the motor thalamus to motor cortical firing and movement is in controlling the trial-to-trial dynamics of cortical activity across different motor cortical areas. It may also be the case that the CTC system facilitates the primary motor cortex while silencing the preparatory PM activity and thus acts as a signal for a rapid transition between motor planning (carried by premotor signals) and motor execution (mediated by the primary motor cortex).

Materials and Methods

Behavioral Task. Data were obtained from three *Macaca fascicularis* monkeys (females, 4.5 to 8 kg). All care and surgical procedures were in accordance with the Hebrew University Guidelines for the Use and Care of Laboratory

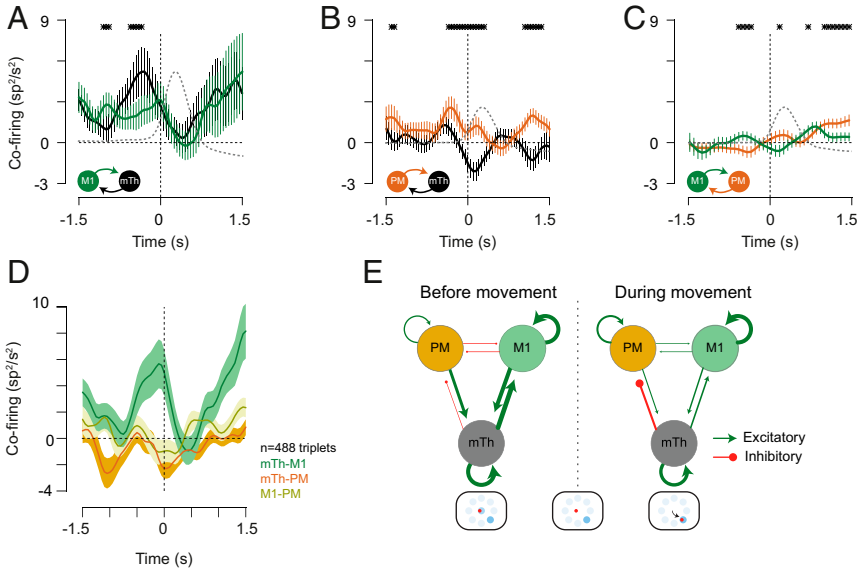

Fig. 4. Analysis of direction-specific TC interactions. (*A*) The mean diagonal of the jPSTHs in Fig. 3*A* (±SEM). The mean was computed using the diagonals highlighted in Fig. 3*A* (dashed lines) which span +0.5 s above the main diagonal and −0.5 s below the main diagonal. This was done to capture the directional interactions between the two sites. Asterisks above the curves correspond to time points where the two traces were significantly different (paired *t* test, $P < 0.05$). (*A*, *Inset*) Relationships between the curves and the specific directional interactions (e.g., the green curve corresponds to M1 preceding mTh and the black curve corresponds to mTh preceding M1). The gray dashed trace shows the average hand velocity profile computed during the same time frame. (*B* and *C*) Same as in *A* but for thalamic–PM pairs (*B*) and M1–PM pairs (*C*). (*D*) The zero-lag (i.e., values along the main diagonal in Fig. 3) pairwise cofiring between the different sites computed for simultaneously recorded triplets of cells (one from each site; $n = 488$ triplets). (*E*) Schematic summary of the directional pairwise interaction results. Connecting lines between sites (circles) correspond to the net correlation between the two areas. Arrowheads indicate positive correlation and circles indicate negative correlation. The width of the arrow corresponds to the magnitude of the correlation. Intraareal autocorrelations are shown as well. (*E*, *Left*) Computed for a time window before movement onset (−0.5 s to 0). (*E*, *Right*) Interactions computed after movement onset (0 to +0.5 s). The dashed vertical line depicts movement onset time.

Animals in Research, and supervised by the Institutional Committee for Animal Care and Use. The behavioral task has been described in detail elsewhere (3). Briefly, the three monkeys were trained to sit in a primate chair, wear an exoskeleton (KINARM; BKIN Technologies), and perform a planar, shoulder-elbow reaching task. In this task, the monkeys were instructed to locate a cursor within a central target. After 500 ms, a peripheral target (one of eight that were evenly distributed) appeared and the monkey had to wait until the central target disappeared ("go" signal) and then reach the cued target. If the monkey moved the cursor to the correct target within the predefined time limit it was rewarded with a drop of applesauce. To encourage the monkey to predict the timing of the go signal, we limited the total time it had to reach the peripheral target to 500 ms and inserted a 200-ms grace period before the go signal. Onset of movement within this time frame did not abort the trial.

After training was completed, a recording chamber (21 × 21 mm) was attached to the monkeys' skull above the hand-related area of the motor cortex in a surgical procedure under general anesthesia. After a recovery and retraining period, we recorded motor cortical activity extracellularly.

Insertion of a Chronic Stimulating Electrode into the Superior Cerebellar Peduncle. To insert a chronic stimulating electrode into the ipsilateral SCP, we implanted a small chamber above the estimated insertion point (based on a primate neuro atlas) and used a postsurgery MRI to plan the electrode trajectory. A bipolar concentric electrode (NSEX100; David Kopf Instruments; impedance range of 30 to 60 kΩ) and the evoked intracortical responses to stimulation through the electrode were used to verify its location (3, 12, 13, 25).

SCP Stimulation Protocol. Single-pulse stimuli (biphasic pulses, 200 μs each phase) were applied through the SCP electrode while the monkey performed the task, and neuronal activity was recorded. In each recording site, we applied a set of stimuli consisting of about 200 stimuli that were delivered at 3 Hz at a fixed intensity (ranging from 50 to 300 μA). For the HFS protocol, we applied a train of stimuli delivered at 130 Hz with intensities ranging from 50 to 150 μA. Each train lasted 120 to 180 s (~20 trials).

Electrophysiological Recordings and Cortical Mapping. Glass-coated tungsten electrodes (impedance 300 to 800 kΩ at 1,000 Hz) were inserted through the recording chamber to different motor cortical sites. The signal obtained from each electrode was amplified ($\times 10^4$) and band-pass–filtered online (300 to 6,000 Hz). The signal was then digitized (32 kHz) and saved to disk.

To record thalamic activity, we first identified the location of the motor thalamus based on MRI scans and planned the appropriate trajectory. During the recording session, we advanced one of the four recording electrodes to reach the planned target site. The identity of the thalamic sites was determined by a significant, early response to single-pulse SCP stimulation. The identity of motor thalamic sites was further confirmed by the motor response evoked when stimulating the thalamic sites through the recording electrode (a train of stimuli applied at 333 Hz for 50 ms). Motor responses were observed and documented by the experimentalists at intensities ≤32 μA, with an average intensity of 11 μA.

To test for motor responses, at the end of each recording session we mapped the motor cortical sites by delivering an intracortical train of microstimuli (a train of stimuli applied at 333 Hz for 50 ms at intensities ≤60 μA). The primary motor cortex was identified as the site where the motor response was obtained at a threshold level of ≤15 μA at a distance from the central sulcus of ≤3 mm. Premotor sites were defined as those where a motor response was evoked at higher amplitudes located more than 3 mm anterior to the central sulcus. In some cases, recording sites were located in the somatosensory cortex. These sites were located caudal to the central sulcus and either required high stimulus intensities to produce a motor response or, more often, did not produce any motor response.

Data Analysis.

Stimulus-evoked responses of single neurons. The first step in the offline processing was to remove the stimulation artifacts from the neural signals by subtracting the average profile of the stimulation artifact from the raw signal (25). Subsequently, an offline-sorting method (AlphaSort; Alpha-Omega) was applied on the cleaned signal to extract the spike times of single units. The SCP-evoked responses were calculated for each unit by computing the PSTH in a time window of −50 to +100 ms around the stimulation time using a 1-ms bin size. Significant responses to the stimulation were identified as described previously (3, 12). In brief, for each cell, the background firing was computed in the range of −50 to −10 ms before stimulus onset time. The poststimulation response was tested using two different time windows. Strongly locked early responses within a window of 1 to 8 ms using 1-ms bins were identified by *t* testing the single-trial spikes against the expected counts given the baseline rate level. A second more global test was then carried out in which we again tested the poststimulus firing rate against background firing in a sliding window of 5 ms, shifted in 1-ms steps (1 bin). Significant responses were defined as those that deviated from the background level with a probability of less than 0.01/*n*, where *n* was the number of bins (with a Bonferroni correction to compensate for the fact that each bin was tested several times). We identified excitatory and inhibitory responses in a time frame of 2 to 45 ms by searching for at least 2 successive significant bins for excitatory responses or 7 significant bins for inhibitory responses.

Identifying SCP-responsive sites. To identify SCP-responsive recording sites, we used the raw multiunit activity (filtered at 300 to 6,000 Hz and sampled at 32 kHz), measured its mean absolute value in the time window spanning −50 to 100 ms around stimulation time, and downsampled the data by a factor of 10. We calculated the baseline activity as the average activity recorded in the time from −50 to −10 ms before movement onset. We identified an early excitatory response by considering time bins between 2 and 15 ms after the stimulation and performing a bin-by-bin *t* test against the average baseline activity, at a significance level of $P < 0.01$. A site was considered to have an excitatory response if there were 7 continuous bins (corresponding to ~2 ms) in which the activity was significantly different from the baseline level.

Quantifying the response gain to SCP stimulation. The strength of the single-unit response to SCP stimulation was quantified using a response gain index that was computed in the following manner. For each cell, we computed the baseline firing rate in a time window of −50 to −10 ms before stimulation time and the poststimulation firing rate during a time window of 1 to 10 ms after stimulation time. The response gain was defined as the difference between these two values over their sum. Cells with a weak response to SCP stimulation had a near-zero response gain, whereas cells that were strongly excited had positive gain values and those that were inhibited by the stimulation had negative response gain values.

Task-related response properties of recorded neurons.

1) Preferred direction: For each unit, we computed the tuning function and its PD. The preferred direction was calculated individually for each isolated unit using a resampling method (8) (4,000 repetitions) during the −500 to 500 ms around movement onset.

2) Onset time of the task-related activity: The onset time of neural activity was calculated using the following steps. First, for each neuron, we computed the average perievent time histogram around movement onset (from −1 to +1 s) and subtracted the baseline level computed during the 1-s period preceding the window used for analysis (i.e., −2 to −1 s relative to movement onset time). We then identified the time of maximal rate level and searched for the prepeak time when the response level was below 20% of the maximal response level. This time was defined as the response onset time for each cell.

3) Joint peristimulus time histogram: We captured the modulation of correlated firing between pairs of neurons in relation to specific events by calculating the jPSTH as described in previous studies (16). In short, we first calculated the PSTHs of each cell around the time of movement onset. To avoid overestimation of the cofiring which can result from the varying neural activity when moving to different targets, we only considered trials where the direction of the movement aligned with the PD ±1 target of one of the cells. For thalamocortical pairs, we only considered trials that aligned with the PD of the thalamic cell and, for corticocortical pairs, the PD was selected randomly between the two cells. For cells that did not have a significant PD, we considered the direction where the firing rate was maximal. We then calculated a matrix in which the $(i,j)^{th}$ bin was the count of coincident firing where one neuron fired a spike at the i^{th} bin and the second neuron fired a spike at the j^{th} bin. The single-trial matrices were then summed to produce the $jPSTH_{Raw}$. Subsequently, we estimated the expected count matrix based on the individual movement-related response of each cell. This predicted matrix ($jPSTH_{Predict}$) was the product of the single-neuron PSTH. In this matrix, the $(i,j)^{th}$ bin was equal to $PSTH1(i)*PSTH2(j)$, where PSTH1 and PSTH2 were the movement-related responses of cells 1 and 2, respectively. Finally, we computed the difference matrix by subtracting $jPSTH_{Raw} - jPSTH_{Predict}$. The jPSTH matrices were calculated using a bin size of 1 ms and then smoothed with a two-dimensional Gaussian kernel with an SD of 2 ms and spanning 50 × 50 bins. For the HFS trials, we computed the PSTHs and compensated for saturation times that may occur as a result of the stimulation artifacts (3). In general, the values obtained for HFS trials came from a smaller number of trials compared with the corresponding values obtained for the control trials. To make up for this difference, we used a bootstrap approach and randomly selected a subset of control trials with a matching number of trials as obtained during HFS. We then followed the same approach as described above to compute the jPSTH during HFS.

However, due to the smaller trial numbers, here we used a smoothing kernel of 2.5 ms and a spanning window of 50 × 50 bins.

During reaching, many joints are recruited to perform correct movement. To rule out any bias that might result from differential activation of the different joints during the movement, we only considered pairs of neurons with matching somatotopic mapping. Namely, pairs of neurons that were recorded from sites that elicited response in proximal arm joints (shoulder or elbow) were paired together, and pairs of neurons from sites with distal arm joints mapping (wrist or fingers) were paired together.

Data Availability. Data and code used in this article have been deposited in our GitHub data repository (https://github.com/Motor-Control-Lab-Hebrew-university/Thalamocortical-Paper).

ACKNOWLEDGMENTS. This work was funded by the Israel Science Foundation (ISF-1801/18), the Deutsche Forschungsgemeinschaft (DFG, German Research Foundation Project-ID 431549029 – SFB 1451), the German-Israel Foundation (GIF, Grant I-1224-396.13/2012), the Jerusalem Brain Center (A.N.), the Harry and Sylvia Hoffman Leadership and Responsibility Program (R.M.), and the generous support of the Baruch Foundation (to Y.P.).

1. P. Strick, P. Sterling, Synaptic termination of afferents from the ventrolateral nucleus of the thalamus in the cat motor cortex. A light and electron microscopy study. *J. Comp. Neurol.* **153**, 77–106 (1974).
2. P. L. Strick, Light microscopic analysis of the cortical projection of the thalamic ventrolateral nucleus in the cat. *Brain Res.* **55**, 1–24 (1973).
3. A. Nashef, O. Cohen, R. Harel, Z. Israel, Y. Prut, Reversible block of cerebellar outflow reveals cortical circuitry for motor coordination. *Cell Rep.* **27**, 2608–2619.e4 (2019).
4. B. A. Sauerbrei *et al*., Cortical pattern generation during dexterous movement is input-driven. *Nature* **577**, 386–391 (2020).
5. J. Dacre *et al*, Cerebellar-recipient motor thalamus drives behavioral context-specific movement initiation (2019). dx.doi.org/10.2139/ssrn.3470398. Accessed 14 January 2021.
6. F. P. Chabrol, A. Blot, T. D. Mrsic-Flogel, Cerebellar contribution to preparatory activity in motor neocortex. *Neuron* **103**, 506–519.e4 (2019).
7. Z. Gao *et al*., A cortico-cerebellar loop for motor planning. *Nature* **563**, 113–116 (2018).
8. U. Shalit, N. Zinger, M. Joshua, Y. Prut, Descending systems translate transient cortical commands into a sustained muscle activation signal. *Cereb. Cortex* **22**, 1904–1914 (2012).
9. M. Weinrich, S. P. Wise, The premotor cortex of the monkey. *J. Neurosci.* **2**, 1329–1345 (1982).
10. M. T. Kaufman, M. M. Churchland, S. I. Ryu, K. V. Shenoy, Cortical activity in the null space: Permitting preparation without movement. *Nat. Neurosci.* **17**, 440–448 (2014).
11. J.-Z. Guo *et al*., Cortex commands the performance of skilled movement. *eLife* **4**, e10774 (2015).
12. A. Nashef, O. Cohen, Z. Israel, R. Harel, Y. Prut, Cerebellar shaping of motor cortical firing is correlated with timing of motor actions. *Cell Rep.* **23**, 1275–1285 (2018).
13. A. Nashef, H. Rapp, M. P. Nawrot, Y. Prut, Area-specific processing of cerebellar-thalamo-cortical information in primates. *Biol. Cybern.* **112**, 141–152 (2018).
14. K. Kurata, Activity properties and location of neurons in the motor thalamus that project to the cortical motor areas in monkeys. *J. Neurophysiol.* **94**, 550–566 (2005).
15. P. L. Strick, Activity of ventrolateral thalamic neurons during arm movement. *J. Neurophysiol.* **39**, 1032–1044 (1976).
16. A. M. Aertsen, G. L. Gerstein, M. K. Habib, G. Palm, Dynamics of neuronal firing correlation: Modulation of "effective connectivity." *J. Neurophysiol.* **61**, 900–917 (1989).
17. A. Galvan, X. Hu, Y. Smith, T. Wichmann, Effects of optogenetic activation of corticothalamic terminals in the motor thalamus of awake monkeys. *J. Neurosci.* **36**, 3519–3530 (2016).
18. L. Gabernet, S. P. Jadhav, D. E. Feldman, M. Carandini, M. Scanziani, Somatosensory integration controlled by dynamic thalamocortical feed-forward inhibition. *Neuron* **48**, 315–327 (2005).
19. S. J. Cruikshank, T. J. Lewis, B. W. Connors, Synaptic basis for intense thalamocortical activation of feedforward inhibitory cells in neocortex. *Nat. Neurosci.* **10**, 462–468 (2007).
20. M. Matelli, G. Luppino, L. Fogassi, G. Rizzolatti, Thalamic input to inferior area 6 and area 4 in the macaque monkey. *J. Comp. Neurol.* **280**, 468–488 (1989).
21. F. A. Middleton, P. L. Strick, Basal ganglia and cerebellar loops: Motor and cognitive circuits. *Brain Res. Brain Res. Rev.* **31**, 236–250 (2000).
22. M. M. Halassa, L. Acsády, Thalamic inhibition: Diverse sources, diverse scales. *Trends Neurosci.* **39**, 680–693 (2016).
23. Y.-W. Lam, S. M. Sherman, Functional topographic organization of the motor reticulothalamic pathway. *J. Neurophysiol.* **113**, 3090–3097 (2015).
24. J. W. Crabtree, Functional diversity of thalamic reticular subnetworks. *Front. Syst. Neurosci.* **12**, 41 (2018).
25. R. Ruach, R. Mitelman, E. Sherman, O. Cohen, Y. Prut, An assumption-free quantification of neural responses to electrical stimulations. *J. Neurosci. Methods* **254**, 10–17 (2015).
26. B. Amirikian, A. P. Georgopoulos, Directional tuning profiles of motor cortical cells. *Neurosci. Res.* **36**, 73–79 (2000).